Manuscript Details

Manuscript number	LUMIN_2019_2287
Title	Atomic deciphering of cation exchange mechanism in upconversion nanoparticles
Article type	Research Paper

Abstract

Transition metal ion doping in upconversion nanoparticles (UCNPs) provides an effective way to enhance the luminescence for their wide array of applications. However, the doping sites of transition metal ions have not been comprehensively explored, and commonly assumed that transition metal ions replace the trivalent lanthanides within the lattice. Here we report that cation exchange of transition metal (Mn2+) in β-NaYF4:Yb3+/Er3+ UCNPs occurs through alkaline metal (Na+) replacement, via 2Na+ ↔ Mn2+ + Vacancy reaction. This process distorts the LnF9 polyhedrons and tailors the surrounding environment around the trivalent lanthanides, thereby improving the upconversion intensity from active lanthanides. Further confirmed by core-shell design and spectroscopic study, we prove that the transition–alkaline metal exchange enables both the emission enhancement and transition probability variation of activators.

Keywords	Mn2+；β-NaYF4 nanoparticles；cation exchange；Rietveld refinement
Manuscript category	Up/down conversion, quantum cutting + energy transfer (inorganic ions)

Corresponding Author	Jiajia Zhou
Corresponding Author's Institution	university of technology sydney
Order of Authors	MING GUAN, Maxim Molokeev, Jiajia Zhou

Submission Files Included in this PDF

File Name [File Type]

Cover letter 20191209.docx [Cover Letter]

Manuscript with figures 20191209.docx [Manuscript File]

Conflict of Interest.docx [Conflict of Interest]

To view all the submission files, including those not included in the PDF, click on the manuscript title on your EVISE Homepage, then click 'Download zip file'.

Dear Editor,

We are submitting a manuscript titled "Atomic deciphering of cation exchange mechanism in upconversion nanoparticles" for your consideration to be published in *Journal of Luminescence.*

In this paper, we successfully achieved Mn^{2+} ions cation exchange in β-$NaYF_4$:Yb^{3+}/Er^{3+} UCNPs and observed enhanced emission intensity. For the first time, we atomically decipher the exchange process, that is, the doped Mn^{2+} replace alkaline metal (Na^+) in the lattice through $2Na^+ \leftrightarrow Mn^{2+} + Vacancy$ reaction. This process distorts the LnF_9 polyhedrons and tailors the surrounding environment around the trivalent lanthanides, thereby improving the upconversion intensity from active lanthanides. Further confirmed by core-shell design and spectroscopic study, we prove that the transition–alkaline metal exchange enables both the emission enhancement and transition probability variation of activators. This study opens new design paths for improving the luminescent properties of UCNPs.

This report is both technically practical and scientifically innovative for broad readership of *Journal of Luminescence.* We therefore ask the editors to consider our manuscript for review and publication in your journal.

With best regards,

Dr. Zhou, Jiajia
Lecturer,
UTS-SUStech Joint Research Centre for Biomedical Materials & Devices, Southern University of Science and Technology, Shenzhen 518055, Guangdong, P. R. China

T: +61 426 574 596
Email: jiajia.zhou@uts.edu.au

Considering the importance of this work in advancing the field of upconversion nanotechnology, we suggest the following experts and peers as the reviewers for this work:

1. **Daniel Jaque**
   Universidad Autonoma de madrid, Spain
   E-mail: daniel.jaque@uam.es
   https://zz.glgooo.top/extdomains/sites.google.com/site/fluorescenceimaginggroup/
   Representative work in this field:

   1. Arppe R, Hyppanen I, Perala N, Peltomaa R, Kaiser M, Wurth C, et al. Quenching of the upconversion luminescence of $NaYF_4:Yb^{3+}$, Er^{3+} and $NaYF_4:Yb^{3+}$, Tm^{3+} nanophosphors by water: the role of the sensitizer Yb^{3+} in non-radiative relaxation. *Nanoscale*. **2015**, 7(27):11746-57.
   2. Arppe-Tabbara R, Näreoja T, Nylund S, Mattsson L, Koho S, Rosenholm J, et al. Photon Upconversion Sensitized Nanoprobes for Sensing and Imaging of pH. *Nanoscale*, **2014**, 6837-43.

2. **Guoping Dong**
   South China University of Technology, China
   Email: dgp@scut.edu.cn
   https://www.researchgate.net/scientific-contributions/38813266_Guoping_Dong
   Representative work in this field:

   1. Song E, Ding S, Wu M, Ye S, Xiao F, Dong G, Zhang Q, Temperature-tunable upconversion luminescence of perovskite nanocrystals $KZnF_3:Yb^{3+}$, Mn^{2+}. *Journal of Materials Chemistry C* **2013**, 1 (27), 4209-4215.
   2. Ye S, Li Y, Yu D, Dong G, Zhang Q, Room-temperature upconverted white light from $GdMgB_5O_{10}$: Yb^{3+}, Mn^{2+}. *Journal of Materials Chemistry* **2011**, 21 (11), 3735-3739.

3. **Fan Zhang**
   Fudan University, China
   E-mail: zhang_fan@fudan.edu.cn
   http://nanobiolab.fudan.edu.cn/people.aspx
   Representative work in this field:

1. Li X, Zhang F, Zhao D., Lab on upconversion nanoparticles: optical properties and applications engineering via designed nanostructure. *Chemical Society Reviews* **2015,** *44* (6), 1346-1378.
2. Zhang F, Che R, Li X, Yao C, Yang J, Shen D, Hu P, Li W, Zhao D., Direct imaging the upconversion nanocrystal core/shell structure at the subnanometer level: shell thickness dependence in upconverting optical properties. *Nano letters* **2012,** *12* (6), 2852-2858.

4. Tero Soukka

Department of Biotechnology, University of Turku, Tykistökatu 6, FIN-20520 Turku, Finland

E-mail: riikka.arppe@utu.fi

Representative work in this field:

1. Huang Y, Skripka A, Labrador-Paez L, Sanz-Rodriguez F, Haro-Gonzalez P, Jaque D, et al. Upconverting nanocomposites with combined photothermal and photodynamic effects. *Nanoscale*. **2018**, 10(2):791-9.

2. Vetrone F, Naccache R, Juarranz de la Fuente A, Sanz-Rodriguez F, Blazquez-Castro A, Rodriguez EM, et al. Intracellular imaging of HeLa cells by non-functionalized $NaYF_4$: Er^{3+}, Yb^{3+} upconverting nanoparticles. *Nanoscale*. **2010**, 2(4):495-8.

5. Mingyong Han

Institute of Materials Research and Engineering, Singapore
Email: my-han@imre.a-star.edu.sg
http://www.bioeng.nus.edu.sg/people/

Representative work in this field:

1. Zhang C, Yang L, Zhao J, et al. White-Light Emission from an Integrated Upconversion Nanostructure: Toward Multicolor Displays Modulated by Laser Power[J]. *Angew Chem Int Ed Engl.*, **2015**,54(39):11531-11535.

Atomic deciphering of cation exchange mechanism in upconversion nanoparticles

Ming Guan[†], Maxim S. Molokeev[‖¶], Jiajia Zhou[†*]

[†]*UTS-SUStech Joint Research Centre for Biomedical Materials & Devices, Southern University of Science and Technology, Shenzhen 518055, Guangdong, P. R. China*

[‖]*Laboratory of Crystal Physics, Kirensky Institute of Physics, SB RAS, Krasnoyarsk 660036, Russia*

[¶] *Siberian Federal University, 79 Svobodny Ave., Krasnoyarsk 660041, Russia*

[*]Author to whom correspondence should be addressed: Jiajia.Zhou@uts.edu.au

Abstract: Transition metal ion doping in upconversion nanoparticles (UCNPs) provides an effective way to enhance the luminescence for their wide array of applications. However, the doping sites of transition metal ions have not been comprehensively explored, and commonly assumed that transition metal ions replace the trivalent lanthanides within the lattice. Here we report that cation exchange of transition metal (Mn^{2+}) in β-$NaYF_4$:Yb^{3+}/Er^{3+} UCNPs occurs through alkaline metal (Na^+) replacement, via $2Na^+ \leftrightarrow Mn^{2+} + Vacancy$ reaction. This process distorts the LnF_9 polyhedrons and tailors the surrounding environment around the trivalent lanthanides, thereby improving the upconversion intensity from active lanthanides. Further confirmed by core-shell design and spectroscopic study, we prove that the transition–alkaline metal exchange enables both the emission enhancement and transition probability variation of activators.

Keywords: Mn^{2+}, β-$NaYF_4$ nanoparticles, cation exchange, Rietveld refinement

Introduction

Lanthanide (Ln^{3+}) doped upconversion nanoparticles (UCNPs), featuring by unique luminescent properties including large Stokes shift, tunable emission spectrum and decay lifetime, zero autofluorescence background and high penetration depth into biological tissue, is emerging as a promising light carrier. The UCNPs are attractive in a wide array of applications[1-7], such as graphics imaging and display[8-10], anti-counterfeiting[11, 12], and biological labelling[13-17]. In order to expedite the practical applications of UCNPs, great research efforts have been paid to enhance the upconversion luminescence[18-20]. Tailoring the local crystal field of the Ln^{3+} ions could be an effective strategy. Accordingly, many transition metal ions including Li^+ have been introduced into various UCNPs to modulate their upconversion luminescence[21, 22]. Hong et al. have reported Zn^{2+} doped $NaYF_4$: Yb^{3+}/Er^{3+} UCNPs and found the improvement of the upconversion luminescence[23]. Kim et al. have successfully incorporated Fe^{3+} ions in β-$NaGdF_4$:Yb^{3+}/Er^{3+} UCNPs, which significantly increased the

visible green and red UC emissions[24].

Transition metal Mn^{2+} ion is an interesting species with significantly long lifetime (typically microsecond scale), which has been frequently employed to tune the emission colour or lifetime of $NaLnF_4$ UCNPs[25, 26]. However, the emission intensity probably encounters a decline instead due to the direct doping induced phase transition from hexagonal to cubic[27, 28]. In contrast, cation exchange is an efficient way to introduce Mn^{2+} ions in UCNPs, with constant morphology and crystal phase compared to initial nanoparticles[29-31]. Liu et al. have reported a cation exchange method and for the first time successfully prepared Mn^{2+}-doped β-$NaGdF_4$ UCNPs, in which Gd host is promoted to assist colour modulation through energy migration[32]. To date, the mechanism of such cation exchange of transition metal ions within $NaYF_4$ UCNPs has not been comprehensively explored. Particularly, it has been generally assumed that the transition metal ions replace the Ln^{3+} instead of Na^+ ions within the lattice of UCNPs. However, because of the differences in ionic radius and electronic polarity to the trivalent Ln^{3+} host ions, the Mn^{2+} ions could induce different local substitution in UCNPs.

In this work, we report a successful execution of Mn^{2+} ions cation exchange in β-$NaYF_4$:Yb^{3+}/Er^{3+} UCNPs. We achieve emission intensity enhancement from Y host, and simultaneously this Mn^{2+} ions cation exchange enables red-to-green emission ratio change. We conduct Rietveld refinement to analyse the crystal structure evolution upon exchange, and further link the crystalline analysis to spectroscopic study to decipher the atomic reaction within a nanoparticle. This enables us to clearly understand the exchange process. This suggests a new pathway to alter the symmetry of the crystal field around the activator ions, leading to enhanced upconversion.

Experimental

$YCl_3 \cdot 6H_2O$ (99.99%), $ErCl_3 \cdot 6H_2O$ (99.99%), $YbCl_3 \cdot 6H_2O$ (99.99%), NH_4F (99.99%), NaOH (98%), 1-octadecene (ODE, 90%), oleic acid (OA, 90%), $MnCl_2$ (99.99%) and hydrochloric acid (HCl, 37%) were purchased from Sigma-Aldrich. Toluene (99.5%), ethanol (100%), methanol (100%), were purchased from Chem-Supply (Australia). All reagents were used as received without further purification.

Synthesis of β-$NaYF_4$: Yb^{3+}/Er^{3+} UCNPs

A modified synthesis method is adopted to prepare β-$NaYF_4$:40%Yb^{3+}/2%Er^{3+} UCNPs[33]. In a typical procedure, a methanol solution of 0.58 mmol YCl_3, 0.4 mmol $YbCl_3$, and 0.02 mmol $ErCl_3$ was mixed with 6 ml OA and 15 ml ODE in a 50 mL flask. The mixture was heated at 150 °C under stirring until the solution became clear. After cooling to 50 °C, a methanol solution containing NH_4F (4 mmol) and NaOH (2.5 mmol) was added with vigorous stirring for more than 1 h. Then, the mixed solution was heated to 90 °C ~ 150 °C to evaporate all the residual methanol and water. Finally, the solution was heated to 300 °C and kept there for 1.5 h under argon. After washing with cyclohexane/ethanol, the synthesized nanoparticles were

dispersed in cyclohexane for use. The core-shell β-$NaYF_4$:40%Yb^{3+}/2%Er^{3+} @$NaYF_4$ UCNPs is obtained via an epitaxial grown shell precursor's layer onto the core UCNPs. The shell precursor is prepared following a similar procedure to that just described in synthesizing the core, except experiencing a reaction at 300 °C.

Cation exchange of Mn^{2+} ions in β-$NaYF_4$: Yb^{3+}/Er^{3+} UCNPs

Cation exchange of Mn^{2+} ions in $NaYF_4$:Yb^{3+}/Er^{3+} UCNPs are performed according to a previous report[32]. In a typical process, the as-prepared oleic acid-capped nanoparticles were dispersed in a mixed solution of ethanol (1 mL) and HCl (0.2 M; 1 mL). The mixture was sonicated for 5 min and collected by centrifugation. Subsequently, the resulting products were washed with ethanol/water several times and re-dispersed in water. After that, a stock aqueous solution (0.9 ml; 0.1 mmol) of the as-prepared ligand-free $NaYF_4$: Yb^{3+}/Er^{3+} nanoparticles was mixed with an aqueous solution of $MnCl_2$ (0.1 ml). The resulting mixture was shaken thoroughly and heated at 90 °C for 30 min. Subsequently, the products were collected by centrifugation, washed with water several times, and re-dispersed in water.

Characterization

X-ray diffraction (XRD, D8 Advance diffractometer, Bruker Corporation, Germany, with Cu-Kα and linear VANTEC detector, λ = 0.15406 nm, 40 kV, 30 mA) was used to examine the phase composition. The powder diffraction data for Rietveld analysis were collected in the 2θ range of 5~100° with a step size of 0.02° and counting time of 2~3 s per step. Rietveld refinement was performed using TOPAS 4.2 software. The morphology of the synthesized nanocrystals was characterized using transmission electron microscopy (TEM; Philips CM10 TEM) at an operating voltage of 100 kV. Elemental analysis was acquired by an energy-dispersive X-ray spectroscopy (EDX). The UC luminescence spectra were obtained using of a Fluorolog-Tau3 spectrofluorometer (JobinYvon-Horiba) equipped with an external 980 nm CW diode laser with a pump power density of 500 W/cm^2. The UC nanoparticles were prepared to a concentration of 1 mg/ml for testing. All the measurements were carried out at room temperature.

Results and Discussion

Figure 1a illustrates the designed cation exchange synthetic strategy to produce different concentration of Mn^{2+} ions doped β-$NaYF_4$:Yb^{3+}/Er^{3+} UCNPs. Figure 1b reveals the enhanced UC luminescence properties of these exchanged UCNPs compared to the Mn^{2+}-free sample. We tuned the concentration of $MnCl_2$ during exchange, and labelled the produced UCNPs as Mn^{2+}-less, Mn^{2+}-highly, and Mn^{2+}-ultra-highly doped UCNPs according to 5, 50, and 100 mM Mn^{2+} ions precursors, respectively. Under 980 nm laser excitation, we observed two major UC emission bands in the spectra of all UCNPs. The green emissions centred at 537 and 555 nm originate from the $^2H_{11/2}\rightarrow{}^4I_{15/2}$ and $^4S_{3/2}\rightarrow{}^4I_{15/2}$ transitions of Er^{3+} ions, respectively; the red emission located at 652 nm is attributed to the $^4F_{9/2}\rightarrow{}^4I_{15/2}$ transition of Er^{3+} ions. Clearly, both

of the green and red emission of various UCNPs increase with the adding of Mn^{2+} ions from 0 to 50 mM, and subsequently decrease with the continuous increase of Mn^{2+} to 100 mM (Figure 1c). Under 50 mM Mn^{2+} ions for cation exchange, the sample shows maximum emission intensity, which equals to 2 times as much as the Mn^{2+}-free UCNPs.

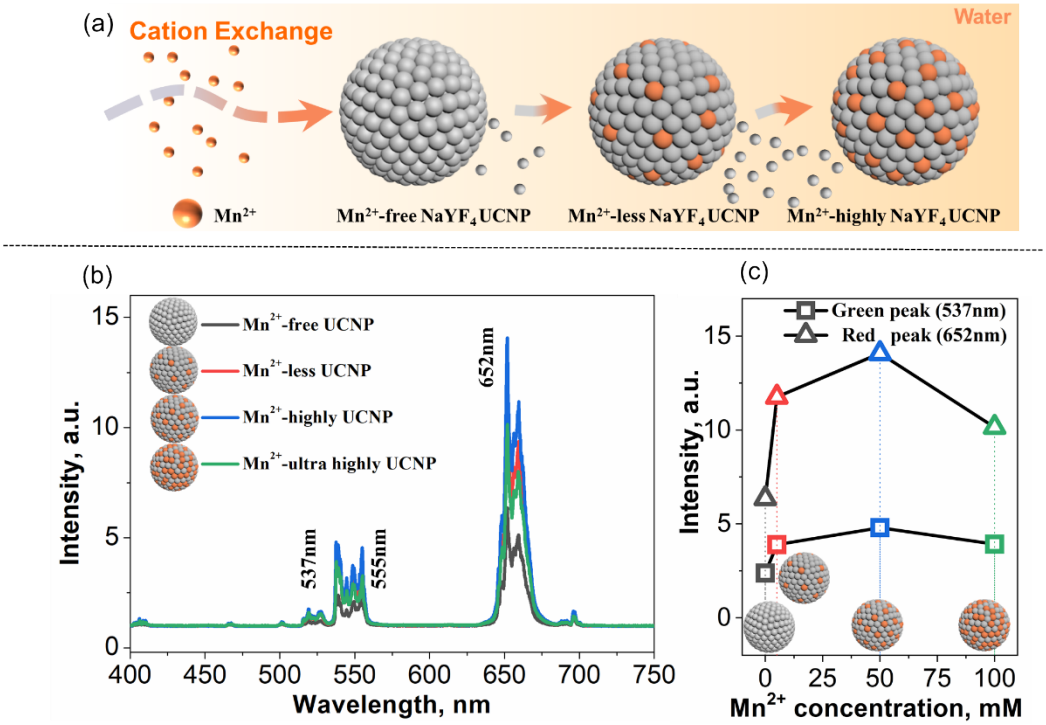

Figure 1 Schematic showing the cation exchange process to produce Mn^{2+} doped β-$NaYF_4$:Yb^{3+}/Er^{3+} UCNPs with different Mn^{2+} concentrations in a aqueous solution (a); UC emission spectra of as-synthesized Mn^{2+}-free, Mn^{2+}-less, Mn^{2+}-highly, and Mn^{2+}-ultra-highly β-$NaYF_4$:Yb^{3+}/Er^{3+} UCNPs (b); Intensity enhancement for green (537 nm) and red (652nm) emission as a function of Mn^{2+} concentration (c).

To confirm the successful exchange, we performed TEM and elemental analysis to check the morphology and ion distribution change of UCNPs after Mn^{2+} exchange. The Mn^{2+}-free UCNPs show spherical-like morphology and uniform distribution of size (Figure 2a). After cation exchange by Mn^{2+} ions, the Mn^{2+}-less and the Mn^{2+}-highly doped UCNPs show negligible changes in terms of crystalline morphology (Figure 2b, c), indicating the preserved size and crystal phase of the UCNPs. Additionally, the elemental mapping result in Figure 2d shows the presence of Mn element on the surface of UCNPs (note the brightness of the image represents the distribution of the Mn^{2+} element). These observations confirm that Mn^{2+} ions successfully penetrated into the surface of UCNPs by cation exchange. To further confirm the entered Mn^{2+} ions locate at the lattice, we performed XRD Rietveld refinement to analyze the crystal structures. In Figure 2e, all the X-ray patterns are in line with the hexagonal $NaYF_4$, indicating that the particle phase did not change after cation exchange. Rietveld refinements, which take $NaYF_4$ (JCPDS card no. 1517675) as starting model, are stable and give low *R*-

factors (Table S1). All thermal parameters show good values (Table S2) and bond distances are in good range (Table S3). In addition, the refined lattice parameters of *a*, *c*, and cell volume of *V* show obvious decreasing trends as a function of Mn^{2+} concentrations (Figure 2f, Table S1). This is due to the smaller ionic radii of Mn^{2+} in coordinate of CN= 6 (IR= 0.83Å) compared to Na^{+} (IR= 1.02Å); and smaller ionic radii of Mn^{2+} in coordinate of CN= 8-9, (IR= 0.96Å, note the maximum coordinate is 8) compared to Y^{3+}(IR= 1.019-1.075Å), Yb^{3+}(IR= 0.985-1.042Å), and Er^{3+} (IR= 1.004-1.062Å). The doping of Mn^{2+} shrinks the unit cells of the UCNPs by replacing Na^{+} or Ln^{3+} ions. The decrease of *a*, *c*, and *V* proves that the Mn^{2+} ions have been exchanged into the lattice, yielding Mn^{2+} doped β-$NaYF_4$:Yb^{3+}/Er^{3+} UCNPs.

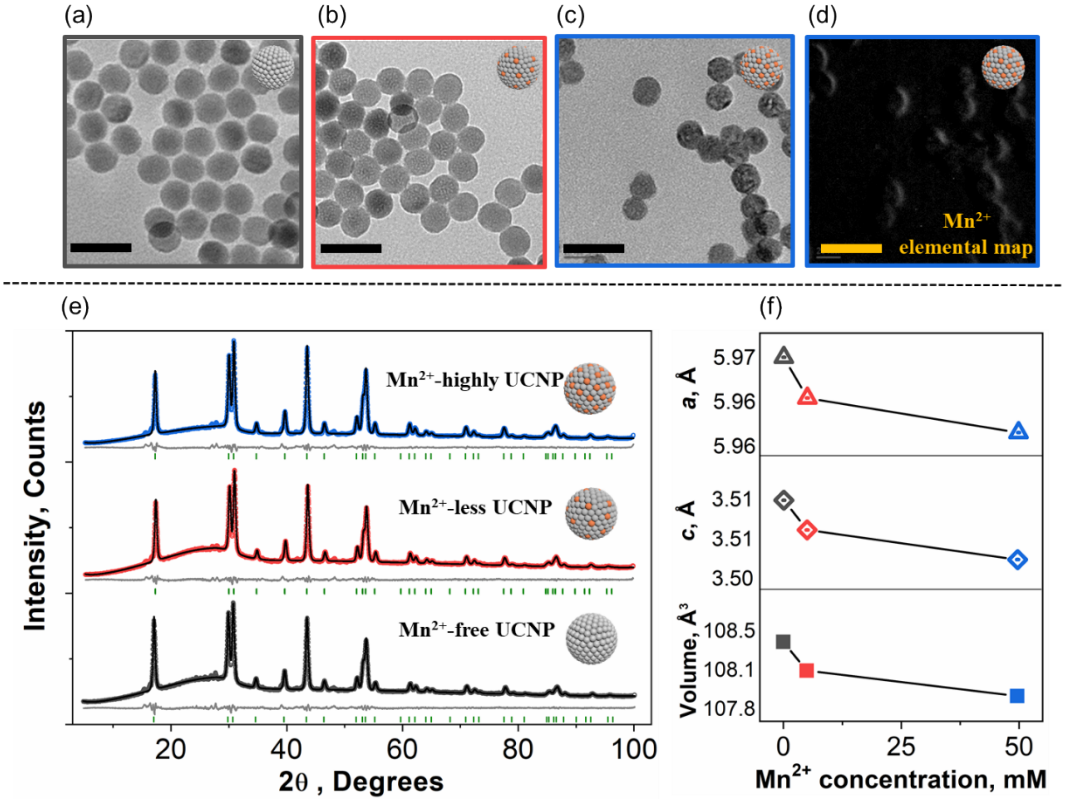

Figure 2 TEM images before and after cation exchange by Mn^{2+} ions: Mn^{2+}-free (a), Mn^{2+}-less (b) and Mn^{2+}-highly doped β-$NaYF_4$:Yb^{3+}/Er^{3+} UCNPs (c); elemental mapping of the Mn^{2+}-highly doped UCNPs, note the brightness represents the concentration of Mn^{2+} element (d); XRD patterns for the refinement of Mn^{2+}-free, Mn^{2+}-less and Mn^{2+}-highly doped UCNPs (e); Refined lattice parameters of a, c, and cell volume (V) showing obvious decreases with increasing Mn^{2+} concentration, indicating Mn^{2+} is doped into the lattice (f). (Scale bar: 50 nm)

In order to atomically decipher the exchange process, we analysed the detailed crystal structures and polyhedrons evolution within these UCNPs. The NaF_6 and LnF_9 polyhedral distortion index, *D*, can be calculated as followed:

$$D = \frac{1}{n}\sum_{i=1}^{n}\frac{|l_i - l_{av}|}{l_{av}} \quad (1),$$

where l_i is the distance between central atom and the ith coordinating atom, and the l_{av} is the mean bond length[34]. These data were shown in Table S3. Figure 3a shows the NaF_6 polyhedron within the Mn^{2+}-doped UCNPs. With the increasing of Mn^{2+} concentration, the average Na^+–F^- bond distances show a dramatic decrease trend (2.34 Å→ 2.33 Å→ 2.31 Å) (Figure 3b), which means that $2Na^+ \leftrightarrow Mn^{2+} + Vacancy$ reaction happens in this crystal system. The replacement of Na^+ by Mn^{2+} induces decrease of the distortion index of $(Na/Mn)F_6$ polyhedron (5.78×10^{-2}→ 5.31×10^{-2}→ 5.01×10^{-2}) (Figure 3c). In contrast, the average Ln^{3+}–F^- bond lengths in LnF_9 polyhedron (Figure 3d) stay almost invariable (2.344 Å→ 2.344 Å→ 2.348 Å) with Mn^{2+} concentration increasing (Figure 3e), which means that Mn^{2+} less likely to occupy the site of Ln^{3+}. However, the LnF_9 polyhedral distortion enlarges (6.29×10^{-3}→ 6.69×10^{-3}→ 7.17×10^{-3}) with the higher doping of Mn^{2+} ions (Figure 3f), which indicates Mn^{2+} ions are strongly disordered over crystal and coordinate with LnF_9 polyhedra. In this case, the Mn^{2+} ions doping by cation exchange makes $(Na/Mn)F_6$ become regular, but the polyhedrons of LnF_9 become more distorted. That is, the $Mn^{2+} \leftrightarrow Na^+$ exchange varies the asymmetric environment, leading to the LnF_9 polyhedral distortion within the lattice of UCNPs. This process tailors the surrounding environment around the Er^{3+} ions in the crystal field, thereby improving the luminescent performance of UCNPs.

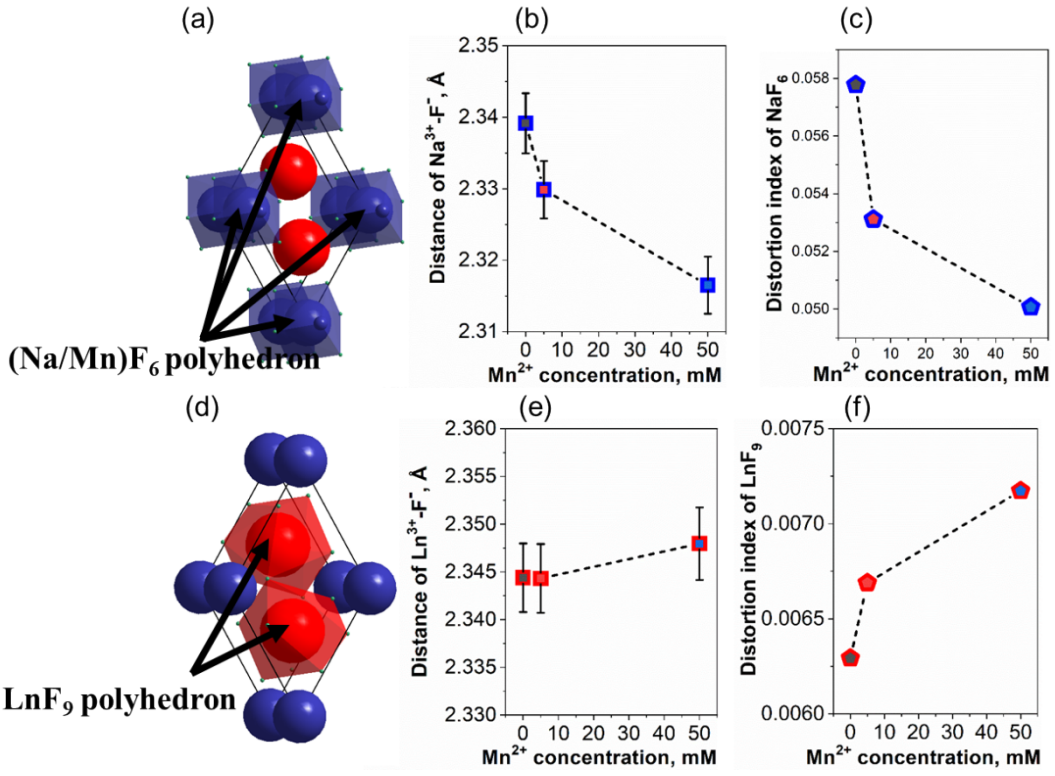

Figure 3 Schematic showing the lattice structure and the NaF_6 polyhedron within the Mn^{2+}-doped UCNPs (a); Calculated Na^+–F^- bond distances (b) and NaF_6 polyhedron distortion indexes (c) showing a decrease trend with increasing Mn^{2+} concentration; Schematic showing LnF_9 polyhedron within the Mn^{2+}-doped UCNPs (d); Calculated average Ln^{3+}–F^- bond lengths stay almost invariable as a function of Mn^{2+} concentration (e); Enlarged LnF_9 polyhedral distortion with increasing Mn^{2+} concentration (f).

The red-to-green emission intensity ratio (I_R/I_G) of Er^{3+} ions is a further evidence of successful incorporation of Mn^{2+} ions in the lattice of β-$NaYF_4$:Yb^{3+}/Er^{3+} UCNPs. To clarify it, we designed core-shell $NaYF_4$:Yb^{3+}/Er^{3+}@$NaYF_4$ UCNPs. The core UCNPs have an average size of 24.1 nm (Figure 4a). The core–shell UCNPs display uniform spherical shape, with an average size of 28.9 nm (Figure 4e), indicating the inert-shell thickness is about 2.5 nm. After cation exchange by Mn^{2+} ions, the I_R/I_G ratio (652/537 nm) in the core $NaYF_4$: Yb^{3+}/Er^{3+} UCNPs gradually increasing from 2.66 in Mn^{2+}-free UCNPs to 3.00 in Mn^{2+}-less UCNPs (or 2.93 in Mn^{2+}-highly UCNPs), as shown in Figure 4b. Due to the existence of Mn^{2+} ions in the lattice, the energy from Yb^{3+} sensitizers was transferred from $^2H_{11/2}$ and $^4S_{3/2}$ levels of Er^{3+} to the $^4T_1$ level of Mn^{2+} through nonradiative energy transfer, followed by further back-energy transfer to the $^4F_{9/2}$ level of Er^{3+} [27, 35, 36]. The Mn^{2+} ions change the transition possibilities of Er^{3+}, and finally facilitate the intensity enhancement of the red emission from $^4F_{9/2}\rightarrow{}^4I_{15/2}$ (Figure 4b, c, d). In contrast, the UC emissions of core-shell $NaYF_4$:Yb^{3+}/Er^{3+}@$NaYF_4$ UCNPs are absence of enhancement after cation exchange by Mn^{2+} ion. In particular, the I_R/I_G ratios of these core-shell samples keep constant, which are determined as 3.25, 3.25 and 3.15 in Mn^{2+}-free, Mn^{2+}-less and Mn^{2+}-highly doped core-shell UCNPs, respectively (Figure 4f). This indicates that the Mn^{2+} exchange in 2.5 nm shell are not able to distort the Er^{3+} site occupancy within the polyhedron structure in the core (Figure 4g). Moreover, only interior doping leads to the efficient energy transfer between Er^{3+} and Mn^{2+}, hence the increased I_R/I_G ratio in core UCNPs testifies the successful cation exchange between Ln^{3+} and Mn^{2+} ions. The penetration depth of cation exchange within UCNPs should be less than 2.5 nm.

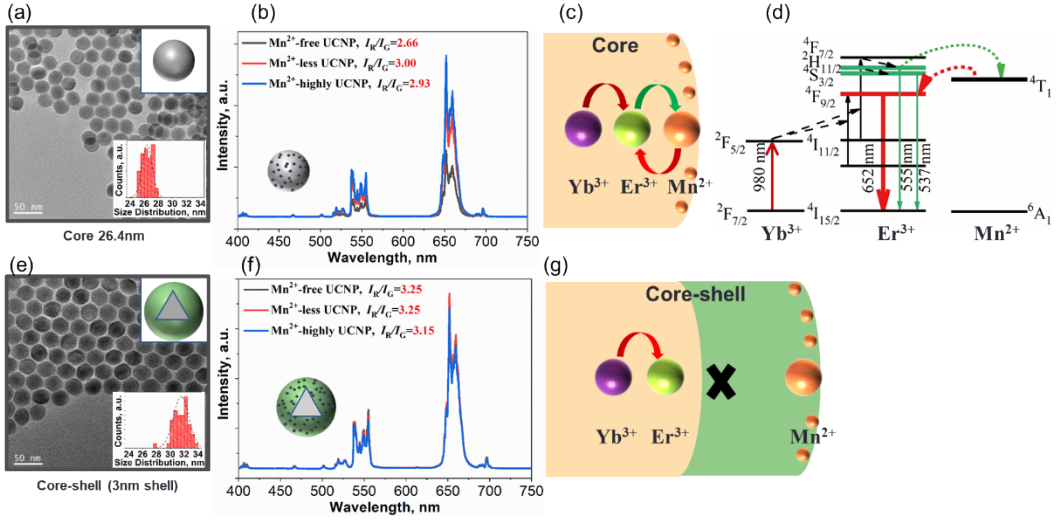

Figure 4 TEM image and size distribution chart of core β-$NaYF_4$:Yb^{3+}/Er^{3+} UCNPs (a); UC spectra and enhanced red-to-green luminescence ratio (IR/IG) in Mn^{2+}-free, Mn^{2+}-less and Mn^{2+}-highly doped core UCNPs (b); Schematic and energy level diagram showing that Mn^{2+} ions disturbed the transition possibilities and facilitated red emission of Er^{3+} in core UCNPs (c, d) ; TEM image and size distribution chart of core-shell β-$NaYF_4$:Yb^{3+}/Er^{3+}@ $NaYF_4$ UCNPs with 2.5nm inert shell (e); UC spectra showing no any I_R/I_G ratio enhancement in Mn^{2+} doped core-shell UCNPs (f); Schematic showing that Mn^{2+} exchanged in 2.5 nm shell are not able to distort the Er^{3+}site occupancy within the polyhedron structure in the core (g).

Conclusions

We have successfully achieved Mn^{2+} ions cation exchange in β-$NaYF_4$:Yb^{3+}/Er^{3+} UCNPs and observed enhanced emission intensity. We have conducted Rietveld refinement to analyse the crystal structure evolution upon exchange, and further link the crystalline analysis to spectroscopic study. For the first time, we atomically decipher the exchange process, that is, the doped Mn^{2+} replace alkaline metal (Na^+) in the lattice through $2Na^+ \leftrightarrow Mn^{2+} + Vacancy$ reaction. In the crystal system, $(Na/Mn)F_6$ polyhedron becomes more regular, while LnF_9 polyhedron becomes more distorted. The LnF_9 polyhedral distortion produced by Mn^{2+} addition tailored the surrounding environment around active lanthanides ions in the crystal field, thereby improving the luminescent performance of UCNPs. Further confirmed by core-shell design and spectroscopic study, we have proven that the $Mn^{2+} \leftrightarrow Na^+$ exchange enables both the emission enhancement and transition probability variation of activator ions. This suggests a new pathway to alter the symmetry of the crystal field around the activator ions, leading to enhanced upconversion luminescence.

Acknowledgements

The authors acknowledge the Australian Research Council (ARC) Discovery Early Career Researcher Award Scheme (J. Z., DE 180100669), and the China Scholarship Council (Ming Guan, No. 201506400025).

References

1. J. Zhou, J. L. Leano, Jr., Z. Liu, D. Jin, K. L. Wong, R. S. Liu and J. G. Bunzli, *Small*, 2018, **14**, e1801882.
2. J. Zhou, S. Wen, J. Liao, C. Clarke, S. A. Tawfik, W. Ren, C. Mi, F. Wang and D. Jin, *Nature Photonics*, 2018, **12**, 154-158.
3. Y. Liu, Y. Lu, X. Yang, X. Zheng, S. Wen, F. Wang, X. Vidal, J. Zhao, D. Liu, Z. Zhou, C. Ma, J. Zhou, J. A. Piper, P. Xi and D. Jin, *Nature*, 2017, **543**, 229-233.
4. S. Wen, J. Zhou, K. Zheng, A. Bednarkiewicz, X. Liu and D. Jin, *Nat Commun*, 2018, **9**, 2415.

5. C.-W. Chen, P.-H. Lee, Y.-C. Chan, M. Hsiao, C.-H. Chen, P. C. Wu, P. R. Wu, D. P. Tsai, D. Tu, X. Chen and R.-S. Liu, *Journal of Materials Chemistry B*, 2015, **3**, 8293-8302.
6. F. Zhang, G. B. Braun, A. Pallaoro, Y. Zhang, Y. Shi, D. Cui, M. Moskovits, D. Zhao and G. D. Stucky, *Nano Lett*, 2012, **12**, 61-67.
7. E. M. Chan, G. Han, J. D. Goldberg, D. J. Gargas, A. D. Ostrowski, P. J. Schuck, B. E. Cohen and D. J. Milliron, *Nano Lett*, 2012, **12**, 3839-3845.
8. X. Liu, Y. Wang, X. Li, Z. Yi, R. Deng, L. Liang, X. Xie, D. T. B. Loong, S. Song, D. Fan, A. H. All, H. Zhang, L. Huang and X. Liu, *Nat Commun*, 2017, **8**, 899.
9. C. Zhang, L. Yang, J. Zhao, B. Liu, M. Y. Han and Z. Zhang, *Angew Chem Int Ed Engl*, 2015, **54**, 11531-11535.
10. R. Arppe, T. Nareoja, S. Nylund, L. Mattsson, S. Koho, J. M. Rosenholm, T. Soukka and M. Schaferling, *Nanoscale*, 2014, **6**, 6837-6843.
11. Y. Lu, J. Zhao, R. Zhang, Y. Liu, D. Liu, E. M. Goldys, X. Yang, P. Xi, A. Sunna, J. Lu, Y. Shi, R. C. Leif, Y. Huo, J. Shen, J. A. Piper, J. P. Robinson and D. Jin, *Nature Photonics*, 2013, **8**, 32-36.
12. J. Zhao, D. Jin, E. P. Schartner, Y. Lu, Y. Liu, A. V. Zvyagin, L. Zhang, J. M. Dawes, P. Xi, J. A. Piper, E. M. Goldys and T. M. Monro, *Nat Nanotechnol*, 2013, **8**, 729-734.
13. Y. Zhong, Z. Ma, S. Zhu, J. Yue, M. Zhang, A. L. Antaris, J. Yuan, R. Cui, H. Wan, Y. Zhou, W. Wang, N. F. Huang, J. Luo, Z. Hu and H. Dai, *Nat Commun*, 2017, **8**, 737.
14. H. He, C. B. Howard, Y. Chen, S. Wen, G. Lin, J. Zhou, K. J. Thurecht and D. Jin, *Anal Chem*, 2018, **90**, 3024-3029.
15. S. Gai, P. Yang, C. Li, W. Wang, Y. Dai, N. Niu and J. Lin, *Advanced Functional Materials*, 2010, **20**, 1166-1172.
16. F. Vetrone, R. Naccache, A. Juarranz de la Fuente, F. Sanz-Rodriguez, A. Blazquez-Castro, E. M. Rodriguez, D. Jaque, J. G. Sole and J. A. Capobianco, *Nanoscale*, 2010, **2**, 495-498.
17. J. Zhou, Z. Liu and F. Li, *Chem Soc Rev*, 2012, **41**, 1323-1349.
18. W. Zheng, P. Huang, D. Tu, E. Ma, H. Zhu and X. Chen, *Chem Soc Rev*, 2015, **44**, 1379-1415.
19. G. Chen, H. Qiu, P. N. Prasad and X. Chen, *Chem Rev*, 2014, **114**, 5161-5214.
20. M. Haase and H. Schafer, *Angew Chem Int Ed Engl*, 2011, **50**, 5808-5829.
21. G. Y. Chen, H. C. Liu, G. Somesfalean, Y. Q. Sheng, H. J. Liang, Z. G. Zhang, Q. Sun and F. P. Wang, *Applied Physics Letters*, 2008, **92**.
22. Q. Cheng, J. Sui and W. Cai, *Nanoscale*, 2012, **4**, 779-784.
23. T. Cong, Y. Ding, J. Liu, H. Zhao and X. Hong, *Materials Letters*, 2016, **165**, 59-62.

24. P. Ramasamy, P. Chandra, S. W. Rhee and J. Kim, *Nanoscale*, 2013, **5**, 8711-8717.
25. M. Liu, Y. Ye, C. Yao, W. Zhao and X. Huang, *J. Mater. Chem. B*, 2014, **2**, 6626-6633.
26. X. Li, X. Liu, D. M. Chevrier, X. Qin, X. Xie, S. Song, H. Zhang, P. Zhang and X. Liu, *Angew Chem Int Ed Engl*, 2015, **54**, 13510-13515.
27. G. Tian, Z. Gu, L. Zhou, W. Yin, X. Liu, L. Yan, S. Jin, W. Ren, G. Xing, S. Li and Y. Zhao, *Adv Mater*, 2012, **24**, 1226-1231.
28. Z. Wu, M. Lin, S. Liang, Y. Liu, H. Zhang and B. Yang, *Particle & Particle Systems Characterization*, 2013, **30**, 311-315.
29. S. Fan, S. Wang, W. Xu, M. Li, H. Sun and L. Hu, *Journal of Materials Science*, 2016, **52**, 869-877.
30. M. Deng and L. Wang, *Nano Research*, 2014, **7**, 782-793.
31. B. J. Beberwyck, Y. Surendranath and A. P. Alivisatos, *The Journal of Physical Chemistry C*, 2013, **117**, 19759-19770.
32. S. Han, X. Qin, Z. An, Y. Zhu, L. Liang, Y. Han, W. Huang and X. Liu, *Nat Commun*, 2016, **7**, 13059.
33. D. Liu, X. Xu, Y. Du, X. Qin, Y. Zhang, C. Ma, S. Wen, W. Ren, E. M. Goldys, J. A. Piper, S. Dou, X. Liu and D. Jin, *Nat Commun*, 2016, **7**, 10254.
34. K. A. Denault, J. Brgoch, M. W. Gaultois, A. Mikhailovsky, R. Petry, H. Winkler, S. P. DenBaars and R. Seshadri, *Chemistry of Materials*, 2014, **26**, 2275-2282.
35. E.-H. Song, S. Ding, M. Wu, S. Ye, F. Xiao, G.-P. Dong and Q.-Y. Zhang, *Journal of Materials Chemistry C*, 2013, **1**.
36. S. Ye, Y.-j. Li, D.-c. Yu, G.-p. Dong and Q.-Y. Zhang, *Journal of Materials Chemistry*, 2011, **21**.

Conflicts of interest

There are no conflicts to declare.